

Bubble phase at $\nu = 1/3$ for a spinless hollow-core interaction

Grégoire Misguich^{1,2}, Thierry Jolicoeur¹ and Takahiro Mizusaki³

¹ *Université Paris-Saclay, CNRS, CEA, Institut de Physique Théorique, 91191 Gif-sur-Yvette, France*

² *Laboratoire de Physique Théorique et Modélisation, CNRS UMR 8089, Université de Cergy-Pontoise, 95302 Cergy-Pontoise, France and*

³ *Institute of Natural Sciences, Senshu University, Tokyo 101-8425, Japan*

(Dated: November, 2020)

We investigate fractional quantum Hall states for model interactions restricted to a repulsive hard-core. When the hard-core excludes relative angular momentum $m = 1$ between spinless electrons the ground state at Landau level filling factor $\nu = 1/3$ is known to be exactly given by the Laughlin wavefunction. When we exclude relative angular momentum three only, Wòjs, Quinn and Yi have suggested the appearance of a liquid state with non-Laughlin correlations. We study this special hard-core interaction at filling factor $1/3$ on the sphere, torus and cylinder geometry. An analysis of the charged and neutral gaps on the sphere geometry points to a gapless state. On the torus geometry the projected static structure factor has a two-peak feature pointing to one-dimensional density ordering. To clarify the nature of the ground state we perform extended DMRG studies on the cylinder geometry for up to 30 particles. The pair correlation function allows us to conclude that the ground state is a two-particle bubble phase.

I. INTRODUCTION

The quantum Hall effect is a striking phenomenon in condensed matter physics. It appears as a low-temperature anomaly in the transport properties of some two-dimensional electronic systems. For special values of an applied perpendicular magnetic field the longitudinal resistance goes to zero with an activated law as a function of the temperature and at the same time there is a plateau in the Hall resistance. The one-electron spectrum in these special circumstances consists of Landau levels with macroscopic degeneracy separated by the cyclotron energy. Coulomb interactions between electrons inside lowest-lying Landau levels give rise to a family of incompressible liquid states that are responsible for the fractional quantum Hall effect (FQHE). Theoretical understanding of the most prominent state at filling factor $\nu = 1/3$ of the lowest Landau level (LLL) is based on an explicit many-particle wavefunction due to Laughlin¹. The composite fermion (CF) theory of Jain² is also based on explicit wavefunctions and capture successfully many physical properties of other FQHE states. These wavefunctions are however not exact eigenstates of the Coulomb interaction Hamiltonian projected onto the LLL. In the case of the Laughlin state it is known that it is the exact ground state of a hard-core interaction that gives a nonzero energy only to states with relative angular momentum $m = 1$ between spinless electrons³. The physical relevance of the Laughlin state stems from the fact that one can adiabatically follow a path in Hamiltonian space between this special hard-core model and the complete Coulomb interaction, without closing the gap. No such model is known for the Jain CF wavefunctions. The CF theory explains the appearance of the experimentally prominent series of FQHE states observed for filling factors $\nu = p/(2p \pm 1)$ with p a positive integer. However this does not exhaust the observed incompressible states. For example in the LLL for filling factors between $\nu = 1/3$ and $\nu = 2/5$ two-dimensional electron gases with high mobility also exhibit additional fractions at $\nu = 5/13, 4/11$. There is also a fraction with *even* denominator in the second Landau level at $\nu = 5/2$ which may very well be the so-called Pfaffian state^{4,5}. The Laughlin/CF states are built with some Jastrow-like correlation factors giving them the correct low-energy properties. The range of validity of these correlations is not yet known. Wòjs and Quinn^{6,7} have argued that the repulsive potential between electrons should have a special “super-harmonic” dependence on the relative angular momentum.

If we consider that FQHE states between $\nu = 1/3$ and $\nu = 2/5$ are due to condensation of quasiparticles or quasiholes emanating from the parent state at $\nu = 1/3$ then it is not clear what is the effective interaction between the quasiparticles/quasiholes. Notably it may be that they are not of the Laughlin/CF type. Wòjs, Yi and Quinn (WYQ) in a series of work^{8–11} have suggested that there is an incompressible state at filling factor $\nu = 1/3$ with non-Laughlin correlations. They consider a special hard-core Hamiltonian which gives nonzero energy only for two-body states with relative angular momentum (RAM) $m = 3$. This may be called a “hollow-core” model since the most repulsive part of the interaction induced by the RAM $m = 1$ interaction is artificially set to zero. By use of extensive exact diagonalizations on the sphere geometry they have given evidence for a series of states that are fluid-like, e.g. with a ground state with zero total angular momentum, and that have several hallmarks of the previously known FQHE states. This series appears for a specific relationship between the number of electrons N_e and the number of flux quanta through the sphere N_ϕ : $N_\phi = 3N_e - 7$. This is to be contrasted with the series corresponding to the Laughlin state which happens for $N_\phi = 3N_e - 3$. The offset 7 vs 3 in the flux-number of particles is called the shift quantum number and is related to the topological properties of the state. This state, which does not belong to the

CF family, has been proposed^{12–20} as a candidate to describe some of the weaker FQHE states at $\nu = 4/11, 5/13$. No explicit candidate wavefunction is known up to now for the WYQ state. Detailed studies are required to understand whether it is really a new type of FQHE or whether it is a state breaking translation symmetry like a stripe or a bubble phase^{21–24} which are not easily discovered on the sphere geometry. It may also be related to quantum Hall nematic states^{28,29} as proposed in a recent study⁶⁶.

In this paper we study the WYQ hollow-core model by exact diagonalizations using sphere^{3,30} and torus geometry³¹. Since the number of particles we can treat is limited to small values we also use the DMRG algorithm on the cylinder geometry to clarify the nature of the ground state. For filling factor $\nu = 1/3$ we show that the values of gaps extracted from charged and neutral excitations extrapolate smoothly to zero in the thermodynamic limit from sphere calculations if we stick to the special WYQ shift $N_\phi = 3N_e - 7$. This indication of compressibility alone does not however allow us to understand the nature of the ground state. We thus use next the torus geometry where there is no shift and so there is direct competition with the Laughlin-like physics as well as competition with states that break translation invariance like stripe or bubble phases. We find that the LLL-projected static structure factor of the WYQ state has several peaks indicating the tendency to spontaneous breakdown of translation symmetry as is observed in the bubble phase in higher Landau levels. If one uses a rectangular unit cell one observes the appearance of a special wavevector where fluctuations are enhanced, indicative of a tendency to spatial ordering. To clarify the nature of this ordering we next ran DMRG studies in the cylinder geometry on large systems of up to 30 electrons to be reasonably sure to avoid finite size effects. We measure the pair correlation function and conclude that the ground state is a two-electron bubble phase as expected from Hartree-Fock theory for Coulomb interactions in higher Landau levels.

It has been proposed that interactions between CF in the effective second Landau level of the CF theory are modelled after the hollow-core pure V_3 model. Following this idea it means that an incompressible ground state of the hollow-core model would explain incompressibility at electronic filling factor $\nu = 4/11$ after the standard Jastrow factor attachment in composite fermion theory since this filling corresponds to filling $\nu^* = 1 + 1/3$ of the CFs. However it is known that the hollow-core model is not always a good model of composite fermions interactions in the second “Lambda”-Landau-level as stated in Ref.(12). Nevertheless CF diagonalization studies¹² with the pure Coulomb interactions have given evidence for an incompressible state of electrons at filling factor $\nu = 4/11$ that happens with an unconventional shift (the same as proposed by WYQ) for the CFs. Our results mean that to generate a valid incompressible state in this universality class, if it exists, one has to go beyond the simple pure hollow-core model. It remains to be seen whether it is possible to deform the hollow-core model and reach the WYQ universality class.

For filling factor $\nu = 1/5$ there is evidence⁴⁸ for a series of states with $N_\phi = 5N_e - 9$ starting at $N_e = 5$ up to $N_e = 12$ which are isotropic and have zero angular momentum. The shift is again different from that of the Laughlin state at $\nu = 1/5$. This special state when expressed in the standard Fock space basis has only integer coefficients for all the accessible sizes we could reach. This does not happen for the WYQ state which has always nonzero energy. The property of integer coefficients is reminiscent of the Jack polynomials^{32–35} that describe several special states many of them being critical with zero gap in the thermodynamic limit. In the torus geometry the hollow-core Hamiltonian has a set of zero-energy ground states that grows with the system size.

In section II we give the basic formalism for hard-core models of the FQHE. Section III is devoted to the study of the thermodynamic limit of the fraction $\nu = 1/3$ for the hollow-core model on the sphere and on the torus geometry. Section IV gives our findings from DMRG studies in the cylinder geometry and we present results giving evidence for a 2-electron bubble phase. Finally section V presents our conclusions. The appendices contain some findings related to the special state at $\nu = 1/5$.

II. HARD CORE MODELS FOR FRACTIONAL QUANTUM HALL STATES

In this work we consider only spin-polarized electronic systems. In the symmetric gauge defined by the vector potential $\mathbf{A} = (\mathbf{B} \times \mathbf{r})/2$ the LLL basis states can be written as :

$$\phi_k(z) = \frac{1}{\sqrt{2^{k+1}\pi}} z^k e^{-|z|^2/4\ell^2}, \quad (1)$$

where k is a positive integer which is the disk angular momentum of the state, $\ell = \sqrt{\hbar/eB}$ is the magnetic length and $z = x + iy$ is the complex coordinate of the particle. A generic many-body state for N_e electrons is thus of the form :

$$\Psi(z_1, \dots, z_{N_e}) = P(z_1, \dots, z_{N_e}) e^{-\sum_i |z_i|^2/4\ell^2}, \quad (2)$$

where P is an antisymmetric polynomial. Since the exponential factor is universal i.e. does not depend on the precise state we will omit it in what follows. The Laughlin wavefunction is defined as a power of the Vandermonde

determinant :

$$\Psi_L^{(p)} = \Psi_V^m = \prod_{i < j} (z_i - z_j)^p. \quad (3)$$

It describes successfully the FQHE state at $\nu = 1/3$ (resp. $\nu = 1/5$) for $p = 3$ (resp. $p = 5$).

A generic two-body interaction Hamiltonian projected onto the LLL can be written as a sum of projectors onto states of definite relative angular momentum m :

$$\mathcal{H} = \sum_{i < j} \sum_m V_m \hat{P}_{ij}^{(m)}, \quad (4)$$

where m is a non-negative integer and the coefficients V_m are the so-called Haldane pseudopotentials³. The antisymmetry of their wavefunction makes spinless fermions sensitive only to odd values of m . The set of pseudopotentials $\{V_m\}$ thus completely characterizes the projected two-body interactions. For the physically relevant case of the Coulomb interaction the V_m are monotonic and decreasing with large m as $\sim m^{-1/2}$. If we consider the hard-core Hamiltonian \mathcal{H}_1 with $V_1 = 1$ and all other pseudopotentials set to zero $V_m = 0, m > 1$ then \mathcal{H}_1 has many zero-energy eigenstates but the densest such state corresponding to a polynomial of smallest total degree is unique and is given precisely by the Laughlin wavefunction for $p = 3$: $\Psi_L^{(3)}$. Similarly we can construct an Hamiltonian with $\Psi_L^{(5)}$ as its exact densest zero-energy state by taking $\mathcal{H}_1 + \mathcal{H}_3$ where \mathcal{H}_3 has only V_3 nonzero positive pseudopotential. In fact any linear combination with positive coefficients of \mathcal{H}_1 and \mathcal{H}_3 has this property. The pseudopotentials offer a convenient way to parametrize deformations of two-body Hamiltonians. For example the belief that the Laughlin state captures correctly the physics of the Coulomb interacting electrons at filling factor $\nu = 1/3$ is based on numerical studies that tune pseudopotentials from the pure hard-core V_1 model to the Coulomb values. The model we focus on in the paper has only V_3 nonzero and will be called the hollow-core model in what follows.

III. THE WOJS-YI-QUINN SERIES $N_\phi = 3N_e - 7$

A. Sphere study

In this geometry, electrons are constrained to move at the surface of a sphere of radius $R = \ell\sqrt{S}$ with $S = N_\phi/2$ and the LLL basis states are given by :

$$\Phi_M^{(S)} = \sqrt{\frac{2S+1}{4\pi} \binom{2S}{S+M}} u^{S+M} v^{S-M}, \quad M = -S, \dots, +S. \quad (5)$$

where M is a half-integer and we have introduced the elementary spinors :

$$u = \cos(\theta/2) e^{i\gamma/2}, \quad v = \sin(\theta/2) e^{-i\gamma/2}, \quad (6)$$

where θ, γ are spherical coordinates. The basis states form a multiplet of angular momentum $L_{orb} = S$. In this geometry the Laughlin wavefunction can be written as :

$$\Psi_L^{(p)} = \prod_{i < j} (u_i v_j - u_j v_i)^p. \quad (7)$$

The wavefunction Eq. (7) is a singlet of zero total orbital angular momentum since it involves only combinations of factors $u_i v_j - u_j v_i$ which are themselves singlets. We use the spherical geometry in some of our exact diagonalization studies. Hence the eigenstates can be classified by their total angular momentum. On the sphere geometry incompressible FQHE states have distinct characteristic features. Notably the ground state is a singlet of total orbital angular momentum and there is a gap above this ground state which is large with respect to the finite-size spacing typical of higher-lying levels. This is at least the case for the standard Laughlin state at $\nu = 1/3$ in the LLL and many other FQHE states. In the case of the $\nu = 1/3$ state if we add one flux quantum then the ground state becomes an isolated multiplet with $L_{orb} = N_e/2$ which is the quasi-hole. Similarly the quasielectron state involves removal of one flux quantum with respect to the fiducial state following $N_\phi = 3(N_e - 1)$. Wojs, Yi and Quinn⁸ have shown by exact diagonalizations up to 12 electrons for the \mathcal{H}_3 model i.e. with only nonzero pseudopotential V_3 that there is also a series of states with essentially the same spectral signatures as the $\nu = 1/3$ FQHE state but with a distinct relation between flux and number of electrons given by $N_\phi = 3N_e - 7$. Even if there is no clear collective mode resembling

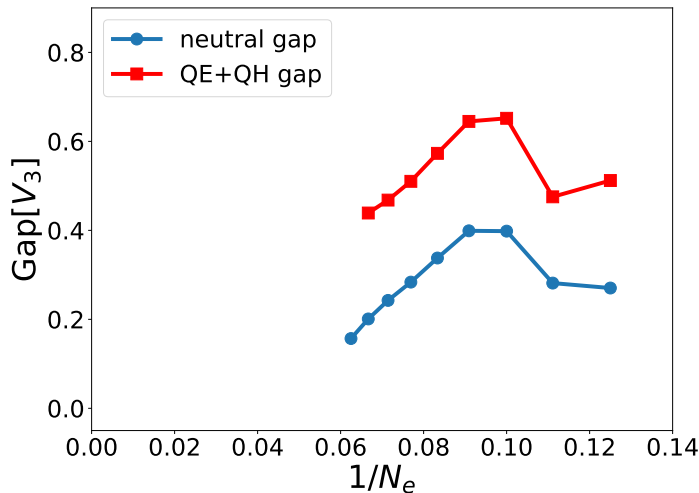


FIG. 1: The gaps for the WYQ sequence of states with $N_\phi = 3N_e - 7$ vs. inverse number of particles. Lower graph gives the neutral excitation gaps defined without change of the flux and the excited state may have any orbital angular momentum. Upper graph gives the quasiparticle-quasihole gap defined through addition/removal of one flux quantum. Sizes range from $N_e = 8$ to 16 in the neutral case and up to $N_e = 15$ in the charged case.

the magnetoroton, the ground state is well separated from higher-lying continuum for all accessible sizes. Taken at face value these results imply the existence of a FQHE state at $\nu = 1/3$ which is topologically distinct from the Laughlin fluid. However one has to check the convergence to the thermodynamic limit. Here we have studied the gap of this system as a function of the number of electrons. The first gap one can define is the lowest excitation energy at $N_\phi = 3N_e - 7$ irrespective of its quantum number. In the standard Laughlin case it is the gap to the minimum of the magnetoroton branch. This neutral gap is displayed in the lower part Fig. (1). One can also define a gap by :

$$\Delta_N = E_0(N_\phi + 1) + E_0(N_\phi - 1) - 2E_0(N_\phi), \quad (8)$$

where $E_0(N_\phi)$ is the ground state of the system with N_e electrons at flux N_ϕ . This gap, when nonzero in the thermodynamic limit, signals a cusp in the energy as a function of density. It is given by the upper curve in Fig. (1). Assuming creation of quasihole/quasielectron by addition/removal of one flux quantum, this quantity is the gap for creating one quasielectron-quasihole pair.

Concerning neutral excitations no amount of fitting can possibly lead to a nonzero value of the gap in the thermodynamic limit since all data points beyond $N_e = 11$ display a downward curvature. Concerning the charged gap Eq. (8) the best linear fit to data beyond $N_e = 11$ leads also to a large negative value of the gap $\approx -0.144V_3$. The best one can do to obtain a positive value is to exclude all data points except the two largest systems and make a linear fit leading to an estimate of $\approx +0.032V_3$ an effect due to the small upward curvature that appears for the largest systems. Since this gap is much smaller than the overall best fit, the best guess is that the charged gap is zero and the state is compressible. Since gap scaling alone may not be a clear signature of the incompressible behavior we turn to the use of DMRG in section IV to access much larger systems. Note that we have not used any rescaling of the magnetic length because this is valid only in the case of Coulomb potential. Indeed when the gap is known to scale as the inverse of the magnetic length it is sensible to correct for the fact that the non-zero shift in the flux-number of particles relation changes the density with respect to thermodynamic limit. However in the case of hard-core models the gap is not proportional to a simple power of ℓ because there is no power-law expression of the potential in real-space.

We note that a scenario in which the charge gap is nonzero but the neutral gap is vanishing corresponds to a quantum Hall nematic phase (see e.g. ref.(49) and references therein). This special state of matter breaks rotation symmetry but respects translation invariance. General microscopic conditions⁴⁹ suggest that one may have to add some extra hard-core components to the Hamiltonian like a V_5 pseudopotential to stabilize it. We will use the pair correlation function in section (IV) to constrain such a possibility.

We have also tried to construct an explicit wavefunction with the WYQ shift. To do so, one has to remove Jastrow-type factors out of the Laughlin wavefunction changing the shift but without changing the total filling factor. A way to do this can be found in the CF construction of wavefunctions. In this theory a composite fermion is a bound state of an electron and two quantized vortices. The vortex attachment reduces the flux felt by the electron and we have

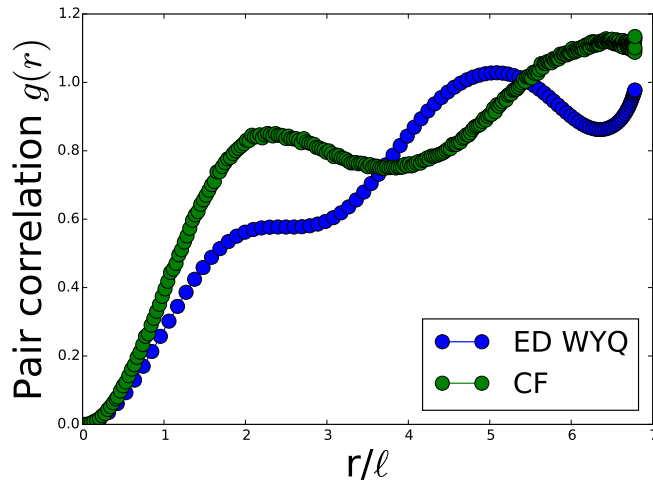


FIG. 2: The pair correlation function obtained from the WYQ state by exact diagonalization of the hollow-core model with $N_e = 10$ fermions is displayed in blue. A composite fermion trial wavefunction with the correct shift and filling factor gives a very different type of correlations : this is the green curve. Both calculations are performed on the sphere geometry.

$N_\phi^* = N_\phi - 2(N_e - 1)$ on the sphere. The particles now occupy effective Landau levels called ALLs and not simply the LLL because they feel this reduced effective magnetic flux. Filling an integer number p of these ALLs leads to the FQHE states at electron filling factor $\nu = p/(2p + 1)$. Implicit in this reasoning is the minimization of some kind of mean-field energy given by the effective cyclotron energy governing the spacing between the ALLs. If we relax this mean-field type of reasoning and just consider the algebraic machinery alone it is possible to fill only an excited Λ level with CFs and to leave empty the lower-lying ALLs. Certainly this is not energetically favorable when using the Coulomb interaction. However it is not immediately clear what happens with the hollow-core \mathcal{H}_3 interaction. This procedure of filling only one higher-lying ALL indeed changes the shift but not the filling factor. If we fill only the second ALL one has a state with shift 5 and filling only the third ALL gives the WYQ shift of 7. Such states are by construction orbital singlets. So we consider a trial wavefunction :

$$\Psi_t = \mathcal{P}_{\text{LLL}} \Phi_2 J^2, \quad (9)$$

where the Jastrow correlation factor J is the Vandermonde determinant on the sphere :

$$J = \prod_{i < j} (u_i v_j - u_j v_i). \quad (10)$$

In this equation Φ_2 is a Slater determinant for the $n = 2$ ALL only and \mathcal{P}_{LLL} is the projection operator onto the LLL. To perform this projection in an efficient way we have used the technique introduced by Jain and Kamilla^{39,40}. By construction this state is an orbital singlet with the WYQ relation between flux and number of particles. We have computed the pair correlation function of this state :

$$g(\vec{r}) = \frac{1}{\rho N_e} \left\langle \sum_{i \neq j} \delta^{(2)}(\vec{r} - \vec{r}_i + \vec{r}_j) \right\rangle \quad (11)$$

where ρ is the density. It may be evaluated by Monte-Carlo sampling. The result is given by the green curve in Fig. (2). The same pair correlation function for the WYQ state obtained from direct exact diagonalization is given by the blue curve in the same figure. While they both have a complex structure they are very different. So we conclude that it is unlikely that the CF wavefunction Eq. (9) can be used to describe the WYQ state at $\nu = 1/3$. Of course this may not exhaust all possibilities of the CF construction.

B. Torus study

The geometry used in ED calculations introduces a bias on the states that can be studied. Notably states with broken space symmetries are frustrated on the sphere and are revealed more clearly on the torus. This is known

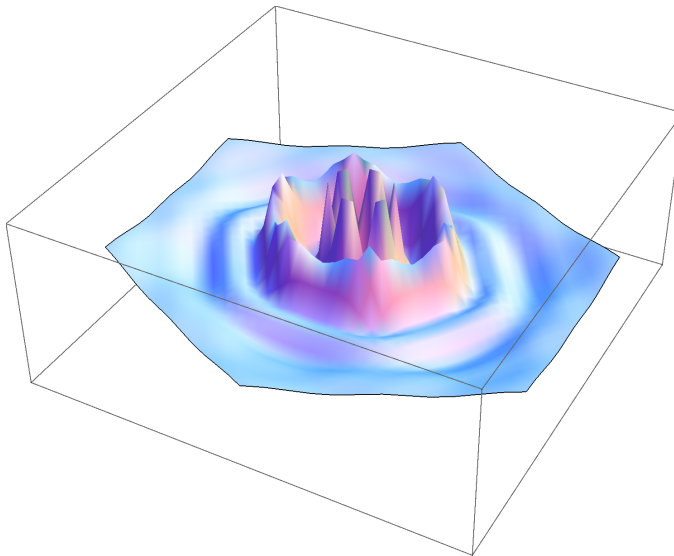


FIG. 3: The projected structure factor $S_0[\mathbf{q}]$ drawn above the basal plane (q_x, q_y) for $N_e = 12$ electrons. The unit cell is hexagonal and the ground state is the WYQ state at filling factor $1/3$. The correlations have a double ring structure with a modulation of sixfold symmetry due to the choice of the unit cell.

to be the case for the stripe states that appear for half-filling in the $N=2$ Landau level and also for the bubble phase for quarter-filling of $N=2$ also^{41–43}. They are identified by a set of quasi-degenerate ground states that form a one-dimensional lattice in momentum space for stripe phases or a 2D lattice for bubble phases.

We have performed exact diagonalizations on the torus geometry using the algebra of magnetic translations which allows us to factor out the overall translation invariance. Eigenstates can be classified by two conserved quantum numbers $s, t = 0, \dots, N_0$ where N_0 is the greatest common divisor (GCD) of N_e and N_ϕ . They correspond to the two-dimensional momenta^{3,31}. We have performed ED studies on the torus up to $N_e = 12$ electrons for the \mathcal{H}_3 model. In the case of a rectangular unit cell by varying the aspect ratio a_0 it is possible to favor states breaking translation invariance. For $0.3 \leq a_0 \leq 1$ there is no evidence for quasi-degenerate states. The ground state remains at $\mathbf{K} = 0$ and as in the sphere case there is no well-defined collective excitation mode before reaching a higher-lying continuum of excited states. In addition to spectral signature an important diagnostic quantity is the LLL-projected static structure factor $S_0(\mathbf{q})$ which can be defined through the guiding center coordinates \mathbf{R}_i :

$$S_0[\mathbf{q}] = \frac{1}{N_e} \sum_{i \neq j} \langle \exp i\mathbf{q}(\mathbf{R}_i - \mathbf{R}_j) \rangle. \quad (12)$$

When evaluated for the stripe or bubble phases it has well-defined peaks in reciprocal space corresponding to the ordering wavevectors. The sensitivity to changes in the shape of the unit is also an indication that the state is compressible. This is what we observe in the case of the WYQ state. The projected structure factor computed in the highly symmetric hexagonal cell is given in Fig. (3). It has a prominent two-ring structure and these rings are not circular, they are sensitive to the boundary conditions and modulated with the symmetry of the unit cell. This is very different from the Laughlin state which has strongly damped oscillations beyond a single central ring surrounding the correlation hole and this ring is insensitive to the shape of the unit cell.

If we distort the cell to a rectangle with aspect ratio 0.4 we find that there are now two well-defined peaks hinting at some form of one-dimensional ordering : see Fig. (4). They persist for $0.3 \lesssim a_0 \lesssim 0.5$. To confirm the spatial pattern we have evaluated the pair correlation function Eq. (11) on the torus geometry. We find that there is a clear pattern that appears. A sample calculation is shown in Fig. (5)

These findings are consistent with a compressible stripe state as the ground state of the WYQ model for filling $\nu = 1/3$. This identification would be complete with the observation of an associated manifold of quasi-degenerate states. Stripe states^{21–24} have been proposed as solutions of the Hartree-Fock approximation for half-filled Landau levels with Coulomb interactions with Landau level index at least 2. The characteristic wavevector of the stripe then decreases with the LL index. Since we do not observe the expected manifold of quasidegenerate states associated with spontaneous breakdown of translation symmetry, it may be that the nature of the ground state is more subtle. Since the number of electrons we consider is quite limited we turn to the DMRG method for the study of larger systems. This study shows that for large enough systems the ground state is indeed a 2-electron bubble phase.

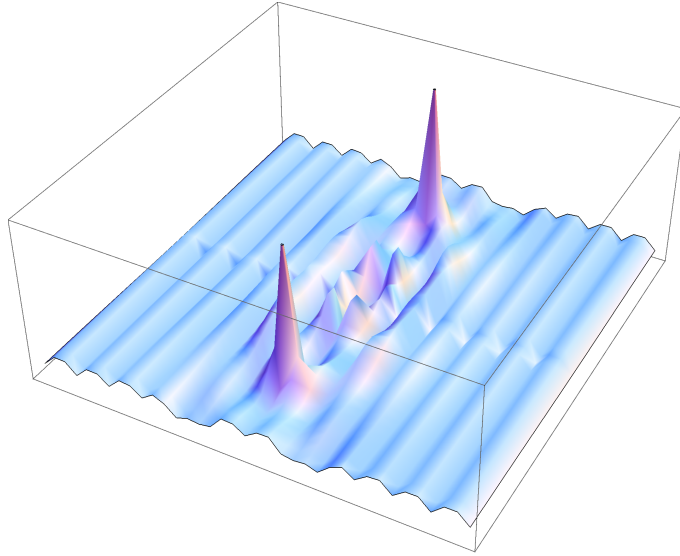


FIG. 4: The projected structure factor $S_0[\mathbf{q}]$ in momentum space in a rectangular unit cell with aspect ratio $a_0 = 0.4$ computed for $N_e = 12$ electrons. There are two sharp peaks suggestive of one-dimensional ordering as confirmed by the real-space calculation of the pair correlation function.

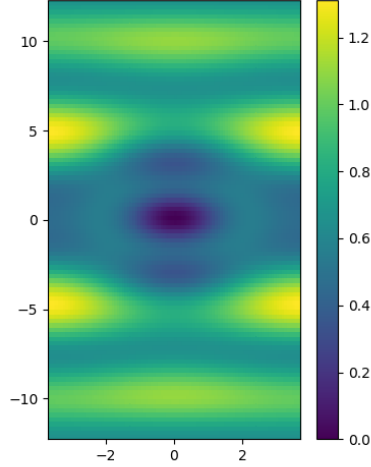


FIG. 5: The pair correlation in real space in a rectangular unit cell with aspect ratio $a_0 = 0.3$ computed for $N_e = 10$ electrons. The reference electron is at the center of the rectangle where it is surrounded by a correlation hole. There are four stripes that are elongated following the smallest dimension of the unit cell. These stripes are separated by a length $\approx 5\ell$.

IV. DMRG STUDY IN THE CYLINDER GEOMETRY

A. Hilbert space

The Hilbert space is the Fock space associated with the lowest Landau orbitals on the cylinder of perimeter L , which are (one-body) wave functions given by :

$$\phi_n(x, y) = \left(\frac{1}{L\ell\sqrt{\pi}} \right)^{\frac{1}{2}} \exp \left(-\frac{1}{2\ell^2} (x - x_n)^2 \right) \exp(ik_n y), \quad k_n = \frac{2\pi n}{L}, \quad x_n/\ell = -\frac{2\pi n}{L/\ell}, \quad (13)$$

where the integer n (positive or negative) labels at the same time the angular momentum k_n in the y direction, and the coordinate x_n of the center of mass of the orbital.

In the following we consider finite cylinders obtained by considering a finite number $N_{\text{orb}} = N_\phi + 1$ of orbitals. The model does not therefore have a sharp boundary in real space. Since the spacing in the x direction between two consecutive orbitals is $\delta x = 2\pi\ell^2/L \rightarrow 2\pi/L$, the length of the cylinder is of order $L_y \simeq N_{\text{orb}}\delta x = 2\pi N_{\text{orb}}\ell^2/L \rightarrow 2\pi N_{\text{orb}}/L$.

For an odd number N_{orb} of orbitals we restrict the index n to be in the range $-(N_{\text{orb}} - 1)/2 \leq n \leq (N_{\text{orb}} - 1)/2$, and for even N_{orb} we take $-N_{\text{orb}}/2 + 1 \leq n \leq N_{\text{orb}}/2$. In the following we will denote by \mathcal{I} this set of integer. The second-quantized form of a generic two-body Hamiltonian reads

$$\mathcal{H} = \frac{1}{2} \sum_{n_1, n_2, n_3, n_4} \mathcal{A}_{n_1, n_2, n_3, n_4} c_{n_1}^\dagger c_{n_2}^\dagger c_{n_3} c_{n_4} \quad (14)$$

where the matrix elements are related to the real space potential $V(r)$ through

$$\mathcal{A}_{n_1, n_2, n_3, n_4} = \int d\mathbf{r}_1 d\mathbf{r}_2 \phi_{n_1}(\mathbf{r}_1)^* \phi_{n_2}(\mathbf{r}_2)^* V(\mathbf{r}_1 - \mathbf{r}_2) \phi_{n_3}(\mathbf{r}_2) \phi_{n_4}(\mathbf{r}_1). \quad (15)$$

We translate the V_1 - V_3 Hamiltonian in the cylinder geometry :

$$\mathcal{H} = \mathcal{H}^{(1)} + \mathcal{H}^{(3)}. \quad (16)$$

with :

$$\mathcal{H}^{(1)} = V_1 \frac{(2\pi)^{5/2}}{L^3} \sum_{b, c, d} (d^2 - c^2) \lambda^{c^2 + d^2} c_{b+c}^\dagger c_{b+d}^\dagger c_{b+c+d} c_b, \quad (17)$$

$$\mathcal{H}^{(3)} = V_3 \frac{(2\pi)^{5/2}}{L^3} \sum_{b, c, d} \lambda^{c^2 + d^2} \left[\frac{3}{2} (d^2 - c^2) + \left(\frac{2\pi}{L} \right)^2 (c^4 - d^4) + \frac{1}{6} \left(\frac{2\pi}{L} \right)^4 (d^6 - c^6) + \frac{1}{2} \left(\frac{2\pi}{L} \right)^4 (c^4 d^2 - c^2 d^4) \right] c_{b+c}^\dagger c_{b+d}^\dagger c_{b+c+d} c_b, \quad (18)$$

where we have defined

$$\lambda = \exp(-2\pi^2\ell^2/L^2) \quad (19)$$

and b, c, d are integers. Only the terms where $b, b+c, b+d$ and $b+c+d$ are in \mathcal{I} are kept. This formulation of the FQHE has already been studied by exact diagonalization^{25–27}. The thermodynamic limit is reached for large number of particles but also by sending L to infinity at the same time. At fixed number of particles the $L \rightarrow 0$ limit, called the thin torus limit as well the “hoop” limit $L \rightarrow \infty$ are pathological.

B. DMRG results

1. Orbital densities

The DMRG results are summarized in Fig. 6 and 7, where the mean orbital occupancies $\langle c_n^\dagger c_n \rangle$ are displayed.

Fig. 6 shows the evolution of the orbital density profile when the Hamiltonian changes from the pure V_1 model to the pure V_3 model, for $N_e = 30$ fermions. At $V_1 = 1$ and $V_3 = 0$ we expect the ground-state to be an incompressible Laughlin state populated/excited with 4 (fractional) quasi-electrons. This is in rough agreement with the density profile displayed in the top panel of Fig. 6 (the homogeneous density of the zero-energy Laughlin state is also displayed for comparison).

When increasing V_3 (and decreasing $V_1 = 1 - V_3$ accordingly) some strong density modulations appear. The number of density maxima (or bumps) evolves as a function of V_3 . This is presumably due to the fact that the optimal separation between the maxima, which would minimize the energy in an infinite system, is evolving continuously with V_3 . But the finite size system has to accommodate a finite number of maxima. For $V_1 = 0.6$ we can identify 7 maxima (including the two on the edges), while this number is only 5 for the hollow-core model ($V_1 = 0$). This shows that inter-maxima distances grow with V_3 . From the present data we can estimate this distance to be around 5.8 magnetic lengths for the hollow-core Hamiltonian $\mathcal{H}^{(3)}$.

It is important to check the robustness of these density modulations with respect to the system size. The upper panel of Fig. 7 displays the orbital occupancies in the pure hollow-core model, and varying number of fermions from 17 to 30 (keeping $N_{\text{orb}} = 3N_e - 6 = N_\phi + 1$). The density modulations appear to be quite robust, showing essentially the same amplitude for 17 and 30 fermions (but a slightly reduced amplitude for $N_e = 20$). We also have a striking similarity between the data for $N_e = 30$ and $N_e = 24$. Concerning the dependence on the perimeter L (at fixed N_e and fixed N_{orb}), the lower panel of Fig. 7 shows that the amplitude of the modulation is almost the same for $L = 20$, 22 and 24. The most elongated cylinder, with $L = 15$, shows some reduced modulations. All these results strongly suggest that the observed modulations are not a spurious finite size effect.

At this stage these modulations could be interpreted in two ways i) as a stripe state or ii) as a crystal state (or bubble crystal) state. In the first case the system would be translation invariant in the y direction, and the stripes would be here rolled up in the periodic direction (y) of the cylinder. In the second scenario, the state would spontaneously break the translation symmetry in both directions in the thermodynamic limit. On a finite system this symmetry necessarily remains unbroken, and the observed stripe-like modulations would come from the fact that the finite-size ground-state is the projection of a broken symmetry state in the $\hat{J} = 0$ sector, hence translation invariant in the y direction. As we will see below, the analysis of the pair correlations allows us to distinguish the two situations and, in the present case, clearly points toward the scenario ii) for the $V_3 = 1$ model.

2. Correlations and signatures of a bubble phase

As discussed in the previous subsection, the orbital occupancies show strong indications of a broken translation symmetry in the x direction. To detect a possible translation symmetry breaking occurring in the y direction too, we now analyze the pair correlations $G(\mathbf{r}_1, \mathbf{r}_2)$, as defined in Eq. (B4).

The results are displayed in Fig. (8). First, panels (a) and (b) show the fermion density $\rho(\mathbf{r})$ in real space for two different system sizes in the pure V_3 model and $N_{\text{orb}} = 3N_e - 6$. These densities are translation invariant in the y direction, as they should be in any eigenstate of J . The strong modulations in the x directions are simply the real-space counterpart of the orbital occupancy modulations described in the previous paragraph.

As for the pair-correlation data, they show some clear triangular pattern of maxima *if the reference point \mathbf{r}_1 lies on a maximum of the density*. This is the case in panels (d) and (e). The number of unit cells of the triangular lattice is 15 in panel (d), with $N_e = 30$ fermions. It is equal to 12 in panel (e), corresponding to a system with 24 fermions. These pair-correlation data should be interpreted as signatures of a bubble phase with two electrons per unit cell. This pattern turns out to be quite robust with the number of fermions and with L , and is already visible on small systems with ~ 10 fermions.

It is also interesting to look at the evolution of the pair correlations as a function of the parameters V_1 and V_3 when the Hamiltonian goes from the pure hollow-core model ($V_1 = 0$ and $V_3 = 1$) to the hard-core one ($V_1 = 1$ and $V_3 = 0$). This is illustrated in Fig. 9. Locating precisely the phase transition(s) along this path goes beyond the scope of this study, but the present data already indicate that the bubble phase should be present at least for $0 \leq V_1/V_3 \leq 0.25$. The nature of the intermediate region where $V_3 \simeq V_1$ would deserve some further study, but the pair correlations displayed in panels (b) and (e) suggest the possibility of a stripe phase which, contrary to the bubble phase, would be translation invariant in the y direction.

Bubble states have already been found numerically using DMRG in higher Landau levels^{51,52}. Our conclusion is related to the results of Ref. 65, which concluded (based on the Hartree-Fock calculations for composite fermions) that bubble states with 2 fermion per cell are energetically favored compared to stripes for the Coulomb interaction and $\nu \lesssim 0.4$. In Ref. 66, based on exact diagonalization, it was claimed that the $V_1 - V_3 - V_5$ model at $\nu = \frac{1}{3}$ realizes a stripe or a smectic state for low V_5 and large V_3 . In view of our results, it seems highly plausible that this phase is in fact nothing but a 2-electron bubble state.

Finally, let us comment on panels (c) and (f) of Fig.(8), where no triangular structure can be seen. They correspond to cases where the reference point is at a density minimum (see panels (a) and (b)), and where the density is in fact close to zero. Forcing a fermion to be there selects particle configurations with a low probability in the many-body wave-function. The fact that the resulting correlation pattern is stripe-like can be interpreted by the fact that picking a low-density point for the reference location does not select (does not “pin”) one broken-symmetry state of the bubble crystal (which is obvious in the limit where the density at the reference points really vanishes).

It is important to note that the pair correlation function we measure indicates a quantum state that breaks both rotation and translation symmetry as expected for a bubble phase. A nematic phase would break only rotation symmetry so its signature would be a correlation hole inside a uniform fluid state but with an asymmetric pattern around this hole, the preferred direction being fixed by the boundary conditions. This is not what we observe here. Indeed when we are closer to the pure V_1 model the pair correlations have a perfectly circular correlation hole and when this phase is destroyed by the effect of V_3 pseudopotential there is appearance of a modulation pattern that

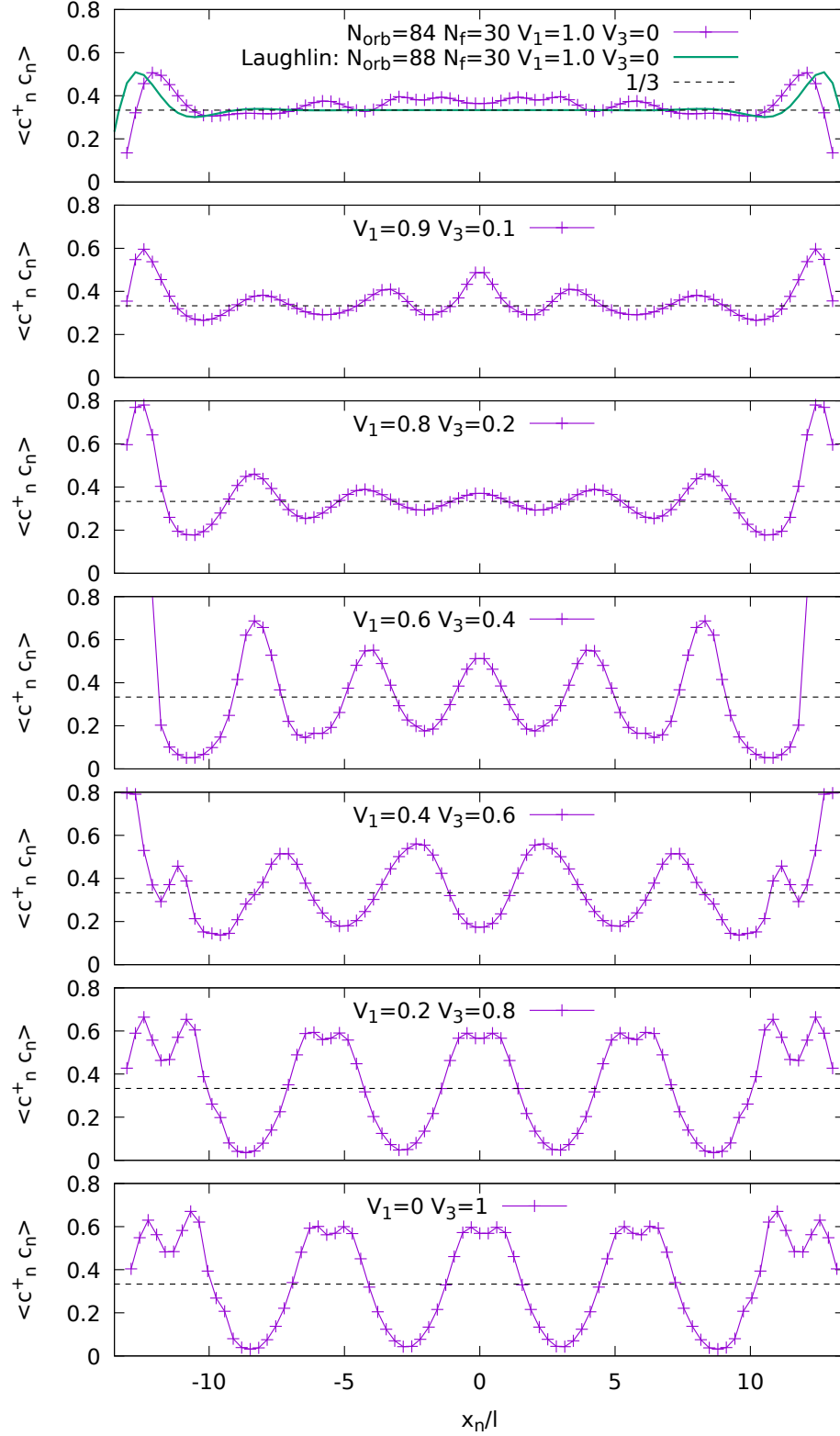


FIG. 6: Orbital occupancies $\langle c_n^\dagger c_n \rangle$ as a function of the (center of mass) coordinate x_n of the n^{th} orbital (in units of the magnetic length ℓ). V_1 varies from 1 to 0 from top to bottom, and $V_3 = 1 - V_1$. Except for the green curve in the top panel (Laughlin state), all data are obtained for $N_e = 30$ fermions in $N_{\text{orb}} = 84$ orbitals ($N_{\text{orb}} = 3N_e - 6 = N_\phi + 1$). All calculations performed with $L = 20$ and $\chi = 8000$. In the top panel we also plotted the orbital densities for the $\nu = 1/3$ zero-energy Laughlin state ($N_{\text{orb}} = 88$). The latter state shows a constant density $n_i \simeq 1/3$ in the bulk of the cylinder. The pair correlations associated with this series of states are displayed in Fig. 9.

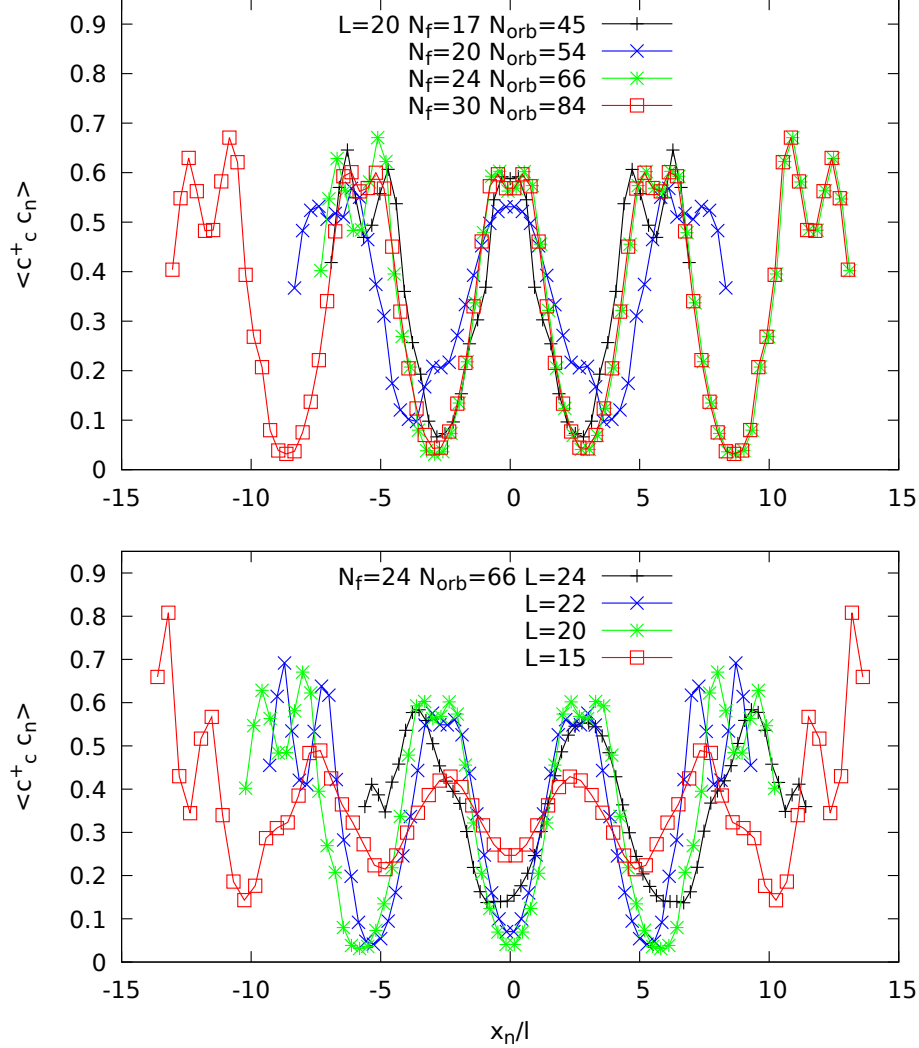


FIG. 7: Orbital occupancies as a function of the position x_n for $V_3 = 1$ $V_1 = 0$ and $N_{orb} = 3N_e - 6$, showing some robust large-amplitude modulations with a period $\simeq 5.8\ell$. Top: Evolution of the density profile with the system size, varying N_{orb} and the number of fermions N_e , keeping $N_{orb} = 3N_e - 6 = N_\phi + 1$ fixed and perimeter $L = 20$. The data for $N_e = 24$ (with a density *minimum* in the center of the cylinder) have been shifted by a half period ($x \rightarrow x + 2.9\ell$), to allow for a comparison with the other system sizes (which have density *maxima* in the center of the system). Bottom: Density profiles for different values of L , with $N_e = 24$ and $N_{orb} = 66$. The data for $L = 24$ has been shifted by a half period ($x \rightarrow x + 2.9\ell$), to allow for a comparison with the other system sizes. Note that the red curve in the upper panel ($N_e = 30$ and $N_{orb} = 84$) is the same as the curve in the bottom panel of Fig. 6.

breaks the translation symmetry in the whole system, well beyond the extent of the hole while a nematic state would have an asymmetric hole surrounded by a uniform background.

V. CONCLUSIONS

We have studied the hollow-core \mathcal{H}_3 model with repulsive interactions only in the RAM $m = 3$ channel at filling fraction $\nu = 1/3$. It has been observed by WYQ that many spectral signatures of an incompressible state are present on the sphere geometry when the shift is taken to be 7. However the scaling of gaps calculated on the corresponding both to neutral and charged excitations points to a compressible state in the thermodynamic limit. This is in agreement with recent calculations on the torus geometry⁶⁶. To clarify the nature of this state we have computed the spatial correlations of the WYQ state on the torus by using the projected static structure factor. For a hexagonal or square

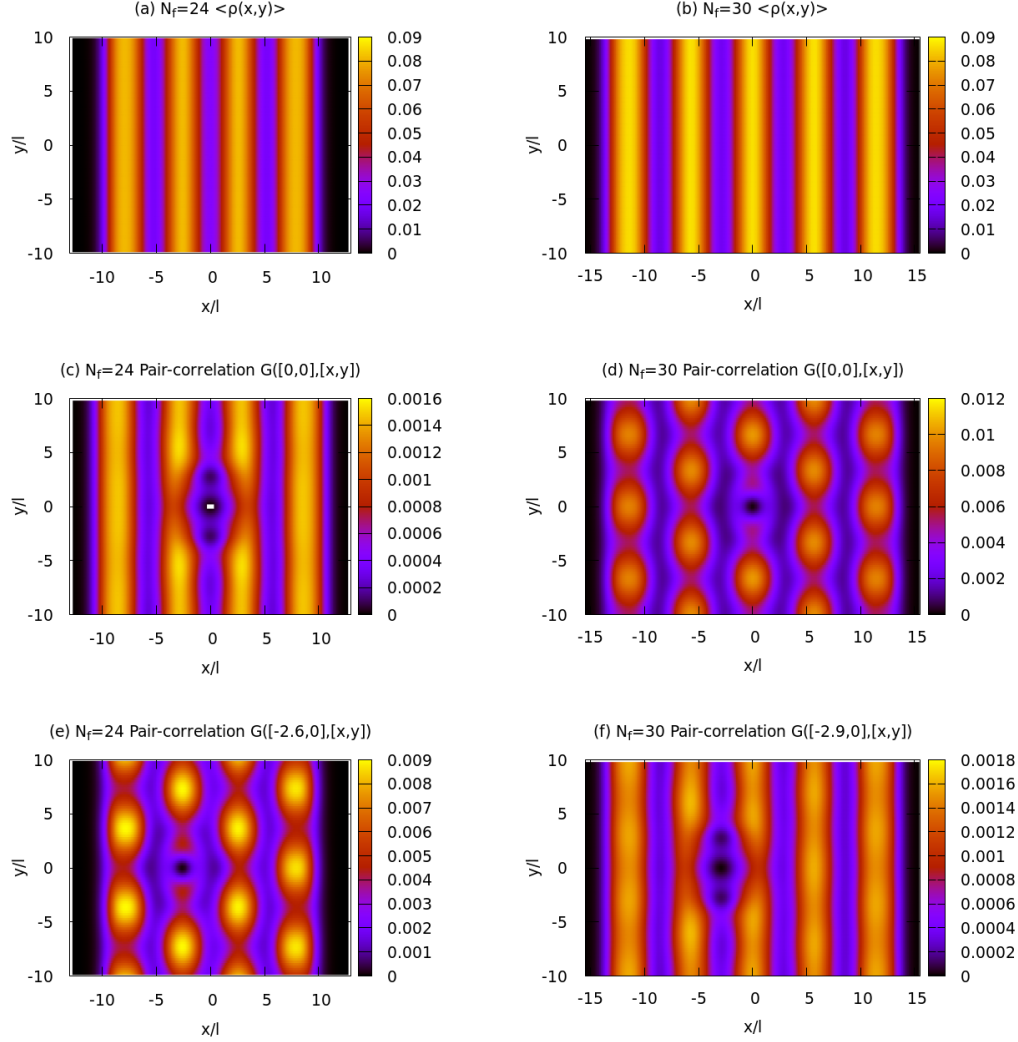


FIG. 8: Density and pair correlations for the hollow-core $\mathcal{H}^{(3)}$ model. (a)-(b) Fermion density $\rho(\mathbf{r})$ (see Eq. A1) (c)-(d) Pair correlation $G(\mathbf{O}, \mathbf{r})$ (see Eq. B4) (e)-(f) Pair correlation $G(\mathbf{r}_1, \mathbf{r})$ with a reference point shifted to the left. (a), (c) and (d): $N_e = 24$ $N_{\text{orb}} = 66$ $L = 20$ (b), (d) and (f): $N_e = 30$ $N_{\text{orb}} = 84$ $L = 20$.

unit cell this quantity has a modulated double-ring structure unlike that of the Laughlin liquid at the same filling factor. When tuning the aspect ratio of a rectangular cell in the range $0.3 \lesssim a_0 \lesssim 0.5$ the structure factor develops two very sharp peaks indicating the presence of a one-dimensional ordering pattern as is the case of half-filled Landau levels of indices $N \geq 2$ for the Coulomb interaction. This is confirmed by computation of the pair correlation in real space in this geometry that shows a stripe modulation with a characteristic length $\approx 5\ell$.

Since these results are severely size-limited we have used the DMRG algorithm on the cylinder geometry to study much larger systems of up to 30 fermions. We have focused again on the pair correlation function to understand the nature of the ground state. While an incompressible ground state would just exhibit a correlation hole and no prominent structure beyond that, we find a clear appearance of a two-dimensional arrangement (for large enough systems beyond those available in the torus or sphere geometry) of modulated density and each overdensity contains exactly two electrons. This is evidence for the 2-electron bubble phase in line with Hartree-Fock theory^{21–24} for Coulomb interaction in higher Landau levels.

In the pair correlation measurements we find evidence for breakdown of both translation and rotation symmetry breaking. This is consistent with a bubble phase but not with a nematic phase that would appear as a uniform state beyond an asymmetric correlation hole. It is likely that one would need to add extra pseudopotentials like V_5 to realize a nematic state⁴⁹.

The bubble phase is compressible in agreement with our findings on gap scaling in the sphere geometry. This

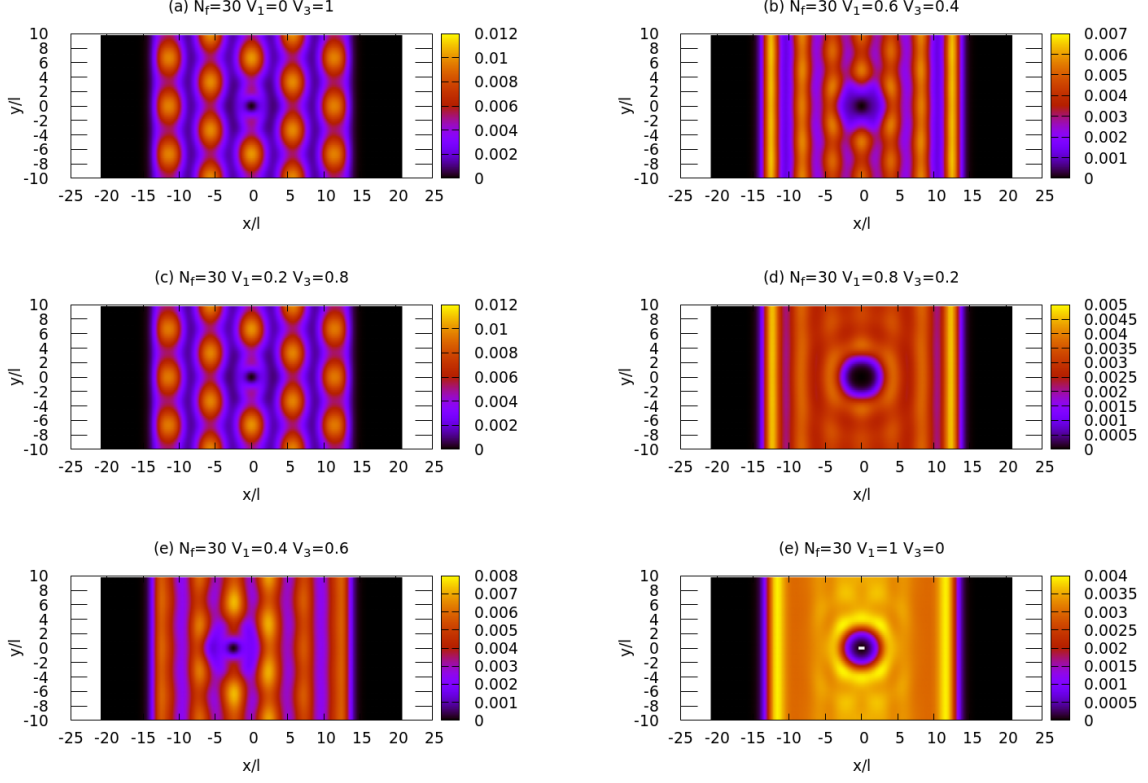


FIG. 9: Pair correlation for the $\mathcal{H}^{(1)}\text{--}\mathcal{H}^{(3)}$ model and different values of V_1 and V_3 (see the legends above each panel). It illustrates the evolution from a bubble state in the hollow-core model [panel(a)] to the Laughlin liquid [in panel (f)] with short-ranged correlations only and an isotropic correlation hole. Note that in the panel (e) the reference point of the pair correlation has been chosen slightly away from the center of the cylinder so that it (approximately) matches a maximum of the density. In all cases $N_e = 30$, $N_{\text{orb}} = 84 = N_\phi + 1$ and $L = 20$, as in Fig. 6.

coherent picture shows that the hollow-core model is not a good candidate for describing the effective theory of composite fermions in the second ΛLL , a remark that was made in Ref. 12. If an unconventional state describes the physics of CF in this case then our results imply that one should go beyond the pure hollow-core model to capture an eventual incompressible phase with the WYQ shift.

Acknowledgments

We acknowledge discussions with O. Golinelli, Ph. Lecheminant and J.-G. Luque. Acknowledgments are also due to E. H. Rezayi and S. H. Simon for useful correspondence. One of us (TJ) thanks J. K. Jain for an interesting discussion. T. M. was supported by the research grant of the Senshu Research Abroad Program (2018). Part of the numerical calculations were performed under the project allocation 100383 from GENCI-IDRIS-CNRS. We also acknowledge CEA-DRF for providing us with CPU time on the supercomputer COBALT at GENCI-CCRT.

Appendix A: First and second-quantized forms of the density in real space

In first-quantized form, the mean density particle density is defined by

$$\rho(\mathbf{r}) = \sum_{i=1}^{N_e} \langle \delta(\mathbf{r} - \hat{\mathbf{r}}_i) \rangle, \quad (\text{A1})$$

where the sum runs over all the particles. In second-quantized form it becomes

$$\rho(\mathbf{r}) = \langle \hat{\psi}^\dagger(\mathbf{r}) \hat{\psi}(\mathbf{r}) \rangle \quad (\text{A2})$$

$$= \sum_{n,n'=1}^{N_{\text{orb}}} \phi_n^*(\mathbf{r}) \phi_{n'}(\mathbf{r}) \langle c_n^\dagger c_{n'} \rangle \quad (\text{A3})$$

$$(\text{A4})$$

where $\hat{\psi}^\dagger(\mathbf{r}) = \sum_n \phi_n^*(\mathbf{r}) c_n^\dagger$ and the sums over n and n' run over all the orbitals (single-particle states). In cases where the total angular momentum is conserved $\langle c_n^\dagger c_{n'} \rangle$ vanishes unless $n = n'$ and one gets

$$\rho(\mathbf{r}) = \sum_n^{N_{\text{orb}}} |\phi_n(\mathbf{r})|^2 \langle c_n^\dagger c_n \rangle \quad (\text{A5})$$

$$= \frac{1}{L\ell\sqrt{\pi}} \sum_n^{N_{\text{orb}}} \exp\left(\frac{(x-x_n)^2}{\ell^2}\right) \langle c_n^\dagger c_n \rangle. \quad (\text{A6})$$

Writing $\mathbf{r} = (x, y)$, the above density is independent of y and gives Eq. C1. The above normalization insures that $\int d^2\mathbf{r} \rho(\mathbf{r}) = \sum_n^{N_{\text{orb}}} \langle c_n^\dagger c_n \rangle = N_e$, as it should.

Appendix B: First and second-quantized forms of the two-point correlations

The density-density correlation function D can be defined as follows :

$$D(\mathbf{r}_1, \mathbf{r}_2) = \sum_{i,j} \langle \delta(\mathbf{r}_1 - \hat{\mathbf{r}}_i) \delta(\mathbf{r}_2 - \hat{\mathbf{r}}_j) \rangle, \quad (\text{B1})$$

where the sum runs over all the particles. In second-quantized form it becomes :

$$D(\mathbf{r}_1, \mathbf{r}_2) = \langle \hat{\psi}^\dagger(\mathbf{r}_1) \hat{\psi}(\mathbf{r}_1) \hat{\psi}^\dagger(\mathbf{r}_2) \hat{\psi}(\mathbf{r}_2) \rangle \quad (\text{B2})$$

$$= \sum_{i,j,k,l=1}^{N_{\text{orb}}} \phi_i^*(\mathbf{r}_1) \phi_j(\mathbf{r}_1) \phi_k^*(\mathbf{r}_2) \phi_l(\mathbf{r}_2) \langle c_i^\dagger c_j c_k^\dagger c_l \rangle. \quad (\text{B3})$$

Another quantity of interest is the pair correlation function :

$$G(\mathbf{r}_1, \mathbf{r}_2) = \sum_{i \neq j} \langle \delta(\mathbf{r}_1 - \hat{\mathbf{r}}_i) \delta(\mathbf{r}_2 - \hat{\mathbf{r}}_j) \rangle, \quad (\text{B4})$$

which, in second quantization gives :

$$G(\mathbf{r}_1, \mathbf{r}_2) = \langle \hat{\psi}^\dagger(\mathbf{r}_1) \hat{\psi}^\dagger(\mathbf{r}_2) \hat{\psi}(\mathbf{r}_2) \hat{\psi}(\mathbf{r}_1) \rangle \quad (\text{B5})$$

$$= \sum_{i,j,k,l=1}^{N_{\text{orb}}} \phi_i^*(\mathbf{r}_1) \phi_j^*(\mathbf{r}_2) \phi_k(\mathbf{r}_2) \phi_l(\mathbf{r}_1) \langle c_i^\dagger c_j^\dagger c_k c_l \rangle. \quad (\text{B6})$$

Appendix C: DMRG implementation

Several authors have employed DMRG simulations to study fractional quantum Hall effect (FQHE) problems^{51–62}. In the present work we performed some matrix-product-state (MPS) and matrix-product operator (MPO) based finite-size DMRG. Our implementation is based on the ITensor⁶³ library.

The Hamiltonian Eqs. 16 is first converted into a matrix-product operator (MPO)⁶⁴. This task is performed using the `AutoMPO` and `toMPO` features of the ITensor library. Although this conversion to an MPO is not exact, in all our calculations the cut-off parameter was set to a very small value, $\epsilon = 10^{-16}$, ensuring that this approximation has no significant effect on the results presented here. Typical values for the bond dimension of the MPO are displayed in Fig. 10 for the $\mathcal{H}^{(1)}$ and $\mathcal{H}^{(3)}$ Hamiltonians.

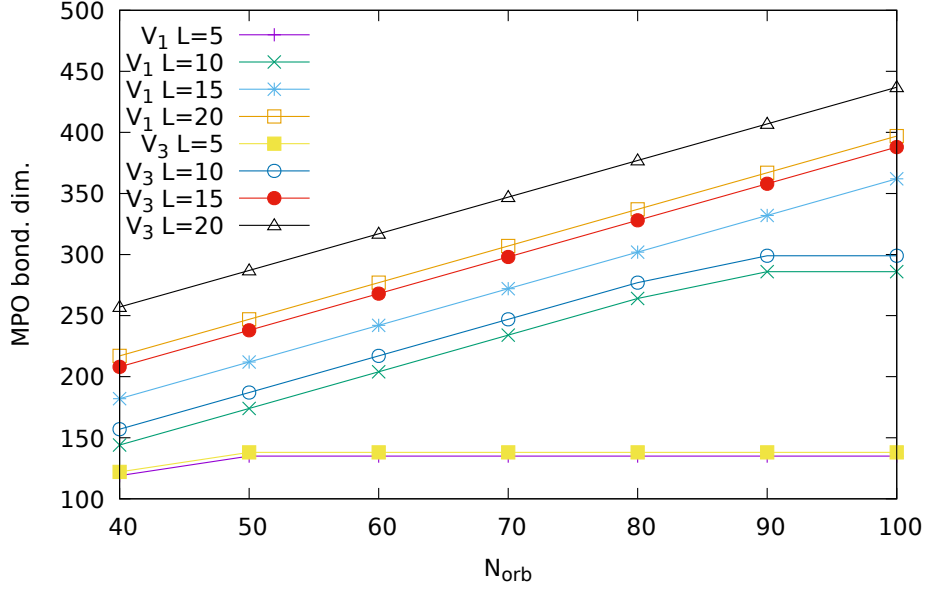


FIG. 10: MPO bond dimension as a function of the number of orbitals, for the V_1 and V_3 models and different values of the perimeter L of the cylinder. The MPO truncation parameter was set to $\epsilon = 10^{-16}$.

For cylinders with an elongated aspect ratio (small L) the parameter λ in Eq. 19 is small and the dominant interactions are relatively short-ranged, and the MPO bond dimension saturates with the cylinder length (parameterized by N_{orb}). This can be observed for $L = 5$ in Fig. 10. On the other hand, for larger L , λ approaches unity and the interactions decay slowly with the orbital separation. In this case the MPO bond dimension increases with L and with N_{orb} . Of course, combining both V_1 and V_3 interactions increases further the bond dimension. As an illustration, for the Hamiltonians used Fig. 6 the bond dimension was found to be between 372 and 389 (depending on the values of V_1 and V_3). For consistency the range of integers c, d in the Hamiltonian should be taken of order L , meaning an increase of complexity when going to the thermodynamic limit.

The code enforces the conservation of two quantum numbers: i) the total number N_e of fermions, and ii) the total angular momentum \hat{J} associated to the periodicity of the cylinder in the y direction. It reads $\hat{J} = \frac{2\pi}{L} \sum_{n \in \mathcal{I}} n c_n^\dagger c_n$ when N_{orb} is odd. When N_{orb} is *even*, however, it is convenient to redefine $\hat{J} = \frac{2\pi}{L} \sum_{n \in \mathcal{I}} (n - \frac{1}{2}) c_n^\dagger c_n$. With this convention the “central” momentum sector, which is the only momentum sector that is invariant under a reflection with respect to plane $x = 0$, is $\hat{J} = 0$ whatever the parity of N_{orb} . All the results discussed here were obtained in this momentum sector. In a few cases we also looked at other momentum sectors to check that the lowest energy state indeed has $\hat{J} = 0$.

To detect some possible inhomogeneous states, we will be interested in the real-space fermionic density $\rho(x, y)$. An eigenstate of total angular momentum \hat{J} is translation invariant in the y direction, and the above density becomes a function of x only. In such a case the density is a convolution of orbital densities $\{\langle c_n^\dagger c_n \rangle\}$ with Gaussians:

$$\rho(x) \sim \sum_n e^{-(x-k_n)^2} \langle c_n^\dagger c_n \rangle. \quad (\text{C1})$$

For this reason most of the information is contained in the orbital densities.

Appendix D: DMRG Convergence

Unless specified otherwise, all the results presented here were obtained with an MPS bond dimension $\chi = 8000$. The number of sweeps we performed typically goes from a few tens to one hundred. This number was determined so that the total energy variation between two successive sweeps is smaller than 10^{-8} .

The Laughlin state is the exact zero-energy ground-state of the pure V_1 model when $N_{\text{orb}} = 3N_e - 2 = N_\phi + 1$ and this provides a simple way to estimate the precision on the energy. With 30 fermions (and $N_{\text{orb}} = 88$) and $L = 20$ we find a (variational) energy $E \simeq 10^{-8}$ and an MPS truncation error $\mathcal{O}(10^{-10})$ for such a state when $\chi = 6000$.

| χ | E_0 | ϵ |
|--------|---------|---------------------|
| 200 | 3.7031 | $7.6 \cdot 10^{-5}$ |
| 1000 | 3.5585 | $1.7 \cdot 10^{-5}$ |
| 2000 | 3.54003 | $6.5 \cdot 10^{-6}$ |
| 4000 | 3.53068 | $3.5 \cdot 10^{-6}$ |
| 6000 | 3.52796 | $1.4 \cdot 10^{-6}$ |
| 8000 | 3.52705 | $9.5 \cdot 10^{-7}$ |

TABLE I: Convergence of the energy as a function of the bond dimension χ . The last column, ϵ , is the largest truncation (discarded weight) during the last sweep. Parameters of the model: $V_1 = 0$, $V_3 = 1$, $N_{\text{orb}} = 84 = N_\phi + 1$, $N_e = 30$ and $L = 20$.

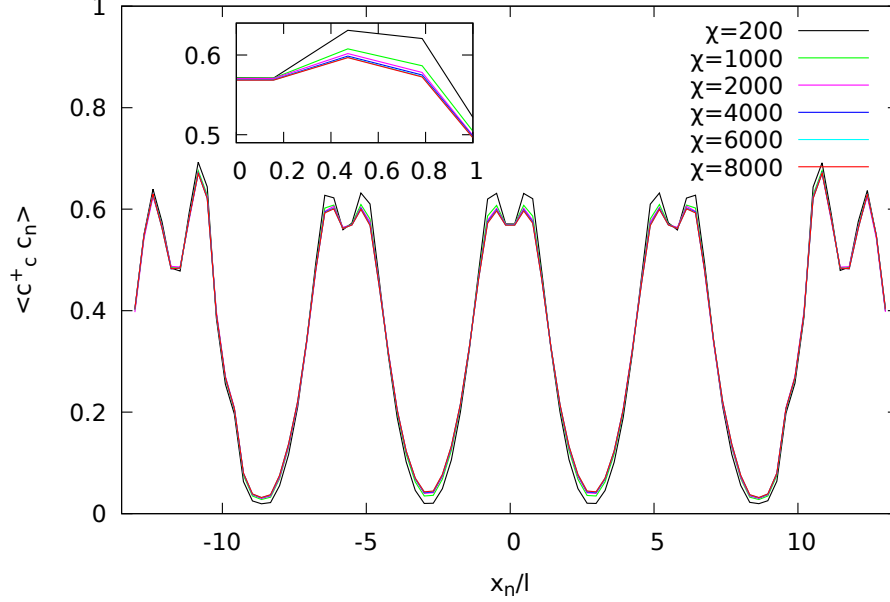


FIG. 11: Orbital occupancies $\langle c_n^\dagger c_n \rangle$ as a function of the (center of mass) coordinate x_n of the n^{th} orbital (in units of the magnetic length l). The different curves correspond to different maximal MPS bond dimension χ , from $\chi = 200$ up to $\chi = 8000$. The curves for $\chi = 2000, 4000, 6000$ and 8000 are almost on top of each other at this scale. The inset shows a zoom on a density maximum in the center of the system. The associated energies and truncations are given in Tab. I. Physical parameters: $N_e = 30$, $N_{\text{orb}} = 84 = N_\phi + 1$ and $L = 20$.

For more complicated states than the Laughlin wave-function, such as the ground of a V_1 - V_3 Hamiltonian we however expect some larger amount of quantum entanglement and a larger truncation error for the same MPS dimension. For $L = 20$ and χ of the order of a few thousand, the largest MPS truncation error is of the order of 10^{-6} (see Tab. I).

Finally, we also show in Fig. 11 the evolution of the orbital densities as a function of the MPS bond dimension χ for a system with 30 fermions, $V_3 = 1$, $V_1 = 0$ and $L = 20$. Although the data for $\chi = 200$ are clearly not converged enough, the curves for $\chi = 1000, 2000, 4000, 6000$ and 8000 are very close to each other.

Appendix E: The $\mathcal{H}^{(3)}$ model series of states at $N_\phi = 5N_e - 9$

It has been observed in Ref. (48) that there is a unique zero-energy ground state for the V_3 model satisfying $N_\phi = 5N_e - 9$ starting from $N_e = 5$. We note that multiplication by a Vandermonde square factor leads to a state which has exactly the WYQ relation between flux and number of particles. This state is also an orbital singlet as expected for a fluid state without ordering. This feature exists at least till $N_e = 11$. Contrary to the case of Laughlin wavefunction this peculiar state is not flanked by zero-energy quasiholes when adding one extra flux quantum. Adding one flux quantum leads to a state with orbital momentum $L_{\text{orb}} = N_e/2$ and a very small but nonzero gap. In fact one needs two additional flux quanta to obtain new states with zero-energy which are now degenerate. For an even number of electrons these states are grouped in orbital multiplets with $L_{\text{orb}} = N_e, N_e - 2, N_e - 4, \dots, 0$ each multiplet

appearing exactly once and there are extra states with $L_{orb} = 0$. Apart from the extra singlet states this is what one expects from two-particle states built with elementary quasiholes having $L_{orb} = N_e/2$. When N_e is odd the pattern of states is identical and the lowest total angular momentum of the set of states is now $L_{orb} = 1$.

We now focus on the peculiar properties of the unique zero-energy state at $N_\phi = 5N_e - 9$. Notably we find that the components of the ground state eigenvector are all integers after removing the normalization factors of the spherical basis and writing the state in terms of the disk states Eq. (1). In fact the property of having integer coefficients is true also for small size systems $N_e = 4, N_\phi = 9, 12$ but the Fock spaces are of very small sizes and it may happen that eigenstates are simple. On the contrary the states satisfying $N_\phi = 5N_e - 9$ quickly involve huge Fock spaces with growing number of particles and thus the integer decomposition is a non-trivial property. The statement of integer coefficients is quickly limited by the machine precision used in exact diagonalization. In fact to obtain all integers coefficients one has to use quadruple precision already for the state at $N_e = 6$ and $N_\phi = 21$ which lies in a space of L_z dimension 2137. In Table (II) we give the first coefficients of the state with $N_e = 5$. The left column gives the integers while the right column contains the binary representation of the occupied state in the Slater determinant. Since we are dealing with spinless fermions the occupations numbers are only 0 or 1.

| | |
|---------|-------------------|
| 3364 | 11000000100000011 |
| -13456 | 11000000010000101 |
| 22736 | 11000000001001001 |
| 25984 | 11000000001000110 |
| -21112 | 11000000000110001 |
| -51968 | 11000000000101010 |
| 129920 | 11000000000011100 |
| -13456 | 10100001000000011 |
| 35320 | 10100000100000101 |
| -19488 | 10100000010001001 |
| - 22272 | 10100000010000110 |
| -31668 | 10100000001010001 |
| -77952 | 10100000001001010 |

TABLE II: The first 13 coefficients in the expansion of the unique zero-energy eigenstate of the $\mathcal{H}^{(3)}$ model for $N_e = 5$ and $N_\phi = 23$. The left column gives the integer while the right column gives the binary representation of the occupation numbers of the Slater determinant. There are a total of 252 integer coefficients in the expansion of the state. The root configuration is at the top of the table. These integers are also the coefficients of the decomposition of the bosonic state \mathcal{S} onto the Schur basis.

Starting from $N_e = 6$ particles we find that the polynomial associated with the special state has a dominance property i.e. not all possible occupation number configuration appear in the expansion. Indeed those with nonzero coefficients can be deduced from a root configuration by successive squeezing operations as happens in many known multivariate special polynomials like the Jack polynomials^{32–35,44}. The squeezing operation moves a given particle from angular momentum m_1 to m'_1 , another particle from m_2 to m'_2 with $m_1 < m'_1 \leq m'_2 < m_2$ and keeping the “center of mass” intact $m_1 + m_2 = m'_1 + m'_2$. The root configuration is 11000000(10000)_k00000011 that we note as 110₆(10₄)_k0₆11 in a chemistry-like notation. The Laughlin wavefunction at the same filling factor has also a root configuration but which is (10000)_k1. This root is non-trivial only starting from $N_e = 6$ because for smaller number of particles there are no constraints on the configurations apart from the L_z angular momentum. We have obtained evidence up to $N_e = 11$ a value beyond which the zero coefficients starts to be numerically undistinguishable from the nonzero ones.

To discuss the special dominance structure it is convenient to use also a bosonic wavefunction obtained by factoring out a Vandermonde determinant since the state is antisymmetric :

$$P(z_1, \dots, z_N) = \prod_{i < j} (z_i - z_j) \times \mathcal{S}(z_1, \dots, z_N) \quad (\text{E1})$$

The antisymmetric N-body state is expanded on a Slater determinant basis :

$$P(z_1, \dots, z_N) = \prod_{i < j} (z_i - z_j) \times \mathcal{S}(z_1, \dots, z_N) = \sum_{\{n_i\}} \mathcal{I}_{\{n_i\}} \det[\{z_j^{n_i}\}]. \quad (\text{E2})$$

If we divide out both sides by the Vandermonde determinant we see that the coefficients $\mathcal{I}_{\{n_i\}}$ determine the expansion of the symmetric polynomial \mathcal{S} onto the Schur basis. The root partition for the bosonic polynomial \mathcal{S} is given by :

$$200000100010001 \dots 1000002 \equiv 20_5(10_3)_k 0_5 2 \quad (\text{E3})$$

This is in fact a partitioning of the total degree of the polynomial. For $N_e = 5$ the root function contains the monomial $z_1^0 z_2^0 z_3^6 z_4^{12} z_5^{12}$ and the total degree is $30 = 12 + 12 + 6$. So we have the following partitions :

$$N_e = 5 : \quad [6, 12, 12] \equiv 30 \quad (\text{E4})$$

$$N_e = 6 : \quad [6, 10, 16, 16] \equiv 48 \quad (\text{E5})$$

$$N_e = 7 : \quad [6, 10, 14, 20, 20] \equiv 70 \quad (\text{E6})$$

The total degree of \mathcal{S} is given by $\frac{1}{2}N_e(4N_e - 8)$. It would be interesting to obtain a closed analytic formula for this special state. The numerous known examples^{32–35,44} suggest that this may be possible. However it is not a *bona fide* Jack polynomial since it is known that the rotational invariance of the state constrains both the root partition as well as the parameter defining the Jack.

If now we study the $\mathcal{H}^{(3)}$ model on a torus at filling $1/5$ then we know already that there will be at least one zero-energy state at the center of the Brillouin zone $K = 0$ which is the non-degenerate Laughlin state. However we find more zero-energy states in a complex pattern. For $N_e = 5$ we find that there is a threefold degenerate state at the center of the Brillouin zone and also additional zero-energy states at the zone boundaries : see Table (III)

| K | $(0, 0)$ | $(0, N_e/2)$ | $(N_e/2, 0)$ | $(N_e/2, N_e/2)$ |
|------|----------|--------------|--------------|------------------|
| deg. | x3 | x1 | x1 | x1 |

TABLE III: The quantum numbers of zero-energy eigenstates for the $\mathcal{H}^{(3)}$ model. Here we display the case of $N_e = 5$ particles. The two components of the wavevector \mathbf{K} are given on the first line in units of $2\pi/L_{x,y}$. The calculation has been done in a rectangular unit cell and is insensitive to the aspect ratio.

| K | $(0, 0)$ | $(0, N_e/2)$ | $(N_e/2, 0)$ | $(N_e/2, N_e/2)$ |
|------|----------|--------------|--------------|------------------|
| deg. | x4 | x1 | x1 | x1 |

TABLE IV: location of the zero-energy states for $N_e = 6$ particles. Same definitions as in Table (III).

| K | $(0, 0)$ | $(0, N_e/2)$ | $(N_e/2, 0)$ | $(N_e/2, N_e/2)$ | $(0, N_e/3)$ | $(N_e/3, 0)$ | $(N_e/3, N_e/3)$ |
|------|----------|--------------|--------------|------------------|--------------|--------------|------------------|
| deg. | x7 | x1 | x1 | x1 | x1 | x1 | x1 |

TABLE V: location of the zero-energy states for $N = 7$ particles. Same definitions as in Table (III). There are now states inside the Brillouin zone with zero-energy.

The number of zero-energy states grows with the number of particles in a manner reminiscent of the Haffnian state³⁶. This special wavefunction is related to an irrational conformal field theory and is presumably gapless^{37,38}. There are several quantum Hall states including the Haldane-Rezayi spin-singlet state^{45–47}, the Gaffnian state⁴⁷ that share this property. We have been unable to find an explicit analytic fomula for this special wavefunction. Its very peculiar properties are worth studying. We have learned that similar findings have been obtained by S. H. Simon in unpublished work.

¹ R. B. Laughlin, Phys. Rev. Lett. **50**, 1395 (1983).

- ² J. K. Jain, “Composite Fermions” (Cambridge University Press, Cambridge, England, 2007).
- ³ F. D. M. Haldane, in “The Quantum Hall Effect” (Springer, New York) edited by Prange and Girvin, 1990.
- ⁴ G. Moore and N. Read, Nucl. Phys. **B360**, 362 (1991).
- ⁵ K. Pakrouski, M. R. Peterson, Th. Jolicoeur, V. W. Scarola, C. Nayak, M. Troyer, Phys. Rev. **X5**, 021004 (2015).
- ⁶ A. Wójs and J. J. Quinn, Phys. Rev. **B61**, 2846 (2000).
- ⁷ A. Wójs and J. J. Quinn, Phys. Rev. **B66**, 045323 (2002).
- ⁸ A. Wójs, K.-S. Yi, and J. J. Quinn, Phys. Rev. **B69**, 205322 (2004).
- ⁹ A. Wójs, D. Wodzinski, and J. J. Quinn, Phys. Rev. **B71**, 245331 (2005).
- ¹⁰ John J. Quinn, Arkadiusz Wójs, Kyung-Soo Yi, and George Simion, Physics Reports **481**, 29 (2009).
- ¹¹ George E. Simion and John J. Quinn, Physica E: Low-dimensional Systems and Nanostructures, **41**, 1 (2008).
- ¹² S. Mukherjee, S. S. Mandal, Y.-H. Wu, A. Wojs, and J. K. Jain, Phys. Rev. Lett. **112**, 016801 (2014).
- ¹³ S. Mukherjee, S. S. Mandal, A. Wojs, and J. K. Jain, Phys. Rev. Lett. **109**, 256801 (2012).
- ¹⁴ S. Mukherjee, J. K. Jain, and S. S. Mandal, Phys. Rev. **B90**, 121305(R) (2014).
- ¹⁵ S. Mukherjee and S. S. Mandal, Phys. Rev. Lett. **114**, 156802 (2015).
- ¹⁶ S. Mukherjee and S. S. Mandal, Phys. Rev. **B92**, 235302 (2015).
- ¹⁷ A. C. Balram, C. Töke, A. Wojs, and J. K. Jain, Phys. Rev. **B91**, 045109 (2015).
- ¹⁸ A. C. Balram, C. Töke, A. Wojs, and J. K. Jain, Phys. Rev. **B92**, 205120 (2015).
- ¹⁹ A. C. Balram, Y.-H. Wu, G. J. Sreejith, A. Wojs, and J. K. Jain, Phys. Rev. Lett. **110**, 186801 (2013).
- ²⁰ J. A. Hutasoit, A. C. Balram, S. Mukherjee, Y. H. Wu, S. S. Mandal, A. Wojs, V. Cheianov, and J. K. Jain, Phys. Rev. **B95**, 125302 (2017).
- ²¹ A. A. Koulakov, M. M. Fogler, and B. I. Shklovskii, Phys. Rev. Lett. **76**, 499 (1996).
- ²² M. M. Fogler, A. A. Koulakov, and B. I. Shklovskii, Phys. Rev. **B54**, 1853 (1996).
- ²³ M. M. Fogler and A. A. Koulakov, Phys. Rev. **B55**, 9326 (1997).
- ²⁴ R. Moessner and J. T. Chalker, Phys. Rev. **B54**, 5006 (1996).
- ²⁵ P. Soulé and Th. Jolicoeur, Phys. Rev. **B85**, 155116 (2012).
- ²⁶ P. Soulé and Th. Jolicoeur, Phys. Rev. **B86**, 115214 (2012).
- ²⁷ P. Soulé, Th. Jolicoeur and Ph. Lecheminant, Phys. Rev. **B88**, 235107 (2013).
- ²⁸ S. A. Kivelson, E. Fradkin, and V. J. Emery, Nature (London) **393**, 550 (1998).
- ²⁹ E. Fradkin and S. A. Kivelson, Phys. Rev. **B59**, 8065 (1999).
- ³⁰ G. Fano, F. Ortolani, and E. Colombo, Phys. Rev. **B34**, 2670 (1986).
- ³¹ F. D. M. Haldane, Phys. Rev. Lett. **55**, 2095 (1985).
- ³² B. A. Bernevig and F. D. M. Haldane, Phys. Rev. Lett. **100**, 246802 (2008).
- ³³ B. A. Bernevig and F. D. M. Haldane, Phys. Rev. **B77**, 184502 (2008).
- ³⁴ B. A. Bernevig and F. D. M. Haldane, Phys. Rev. Lett. **101**, 246806 (2008).
- ³⁵ B. A. Bernevig and F. D. M. Haldane, Phys. Rev. Lett. **102**, 066802 (2009).
- ³⁶ M. Hermanns, N. Regnault, B. A. Bernevig, and E. Ardonne, Phys. Rev. **B83**, 241302(R) (2011).
- ³⁷ N. Read, Phys. Rev. **B79**, 245304 (2009).
- ³⁸ N. Read, Phys. Rev. **B79**, 045308 (2009).
- ³⁹ J. K. Jain and R. K. Kamilla, Int. J. Mod. Phys. **B11**, 2621 (1997).
- ⁴⁰ J. K. Jain and R. K. Kamilla, Phys. Rev. **B55**, R4895 (1997).
- ⁴¹ F. D. M. Haldane, E. H. Rezayi, and K. Yang, Phys. Rev. Lett. **85**, 5396 (2000).
- ⁴² E. H. Rezayi, F. D. M. Haldane, and K. Yang, Phys. Rev. Lett. **83**, 1219 (1999).
- ⁴³ K. Yang, F. D. M. Haldane, and E. H. Rezayi, Phys. Rev. **B64**, 081301(R) (2001).
- ⁴⁴ B. A. Bernevig, V. Gurarie, and S. H. Simon, J. Phys. A: Math. Theor. **42**, 245206 (2009).
- ⁴⁵ F. D. M. Haldane, E.H. Rezayi, Phys. Rev. Lett. **60**, 956 (1988).
- ⁴⁶ V. Gurarie, M. Flohr, and C. Nayak, Nucl. Phys. **B498**, 513 (1997).
- ⁴⁷ S. H. Simon, E. H. Rezayi, and N. R. Cooper, Phys. Rev. **B75**, 075318 (2007).
- ⁴⁸ A. Wojs, Phys. Rev. **B79**, 041304(R) (2009).
- ⁴⁹ B. Yang, Phys. Rev. Research **2**, 033362 (2020).
- ⁵⁰ S. R. White, Phys. Rev. Lett. **69**, 2863 (1992),
- ⁵¹ N. Shibata and D. Yoshioka, Phys. Rev. Lett. **86**, 5755 (2001),
- ⁵² D. Yoshioka and N. Shibata, Physica E: Low-dimensional Systems and Nanostructures **12**, 43 (2002),
- ⁵³ N. Shibata and D. Yoshioka, J. Phys. Soc. Jpn. **72**, 664 (2003),
- ⁵⁴ A. E. Feiguin, E. Rezayi, C. Nayak, and S. Das Sarma, Phys. Rev. Lett. **100**, 166803 (2008),
- ⁵⁵ D. L. Kovrizhin, Phys. Rev. **B81**, 125130 (2010),
- ⁵⁶ J. Zhao, D. N. Sheng, and F. D. M. Haldane, Phys. Rev. **B83**, 195135 (2011),
- ⁵⁷ M. P. Zaletel, R. S. K. Mong, F. Pollmann, and E. H. Rezayi, Phys. Rev. **B91**, 045115 (2015),
- ⁵⁸ W. Zhu, S. S. Gong, F. D. M. Haldane, and D. N. Sheng, Phys. Rev. Lett. **115**, 126805 (2015),
- ⁵⁹ W. Zhu, S. S. Gong, F. D. M. Haldane, and D. N. Sheng, Phys. Rev. **B92**, 165106 (2015),
- ⁶⁰ S. Johri, Z. Papic, P. Schmitteckert, R. N. Bhatt, and F. D. M. Haldane, New J. Phys. **18**, 025011 (2016), ISSN
- ⁶¹ W. Zhu, Z. Liu, F. D. M. Haldane, and D. N. Sheng, Phys. Rev. **B94**, 245147 (2016),
- ⁶² Z.-W. Zuo, A. C. Balram, S. Pu, J. Zhao, Th. Jolicoeur, A. Wójs, and J. K. Jain, Phys. Rev. **B102**, 075307 (2020),
- ⁶³ ITensor Library, <http://itensor.org> (version 3.1.1), URL <http://itensor.org>.
- ⁶⁴ U. Schollwöck, Annals of Physics **326**, 96 (2011), ISSN 0003-4916,

⁶⁵ S.-Y. Lee, V. W. Scarola, and J. K. Jain, Phys. Rev. B **66**, 085336 (2002),

⁶⁶ N. Regnault, J. Maciejko, S. A. Kivelson, and S. L. Sondhi, Phys. Rev. B **96**, 035150 (2017),